RESEARCH ARTICLE

CrossMark

Ejective and Sweeping Motions Above a Peatland and Their Role in Relaxed-Eddy-Accumulation Measurements and Turbulent Transport Modelling

Gabriel Katul[1,2,3] · **Olli Peltola**[3] · **Tiia Grönholm**[3] · **Samuli Launiainen**[4] · **Ivan Mammarella**[3] · **Timo Vesala**[3,5]

Abstract

The three turbulent velocity components, water vapour (H_2O), carbon dioxide (CO_2), and methane (CH_4) concentration fluctuations are measured above a boreal peatland and analyzed using conditional sampling and quadrant analysis. The overarching question to be addressed is to what degree lower-order cumulant expansion methods describe transport efficiency and the relative importance of ejections and sweeps to momentum, CH_4, CO_2 and H_2O fluxes across a range of atmospheric flow regimes. The patchy peatland surface creates distinctly different source and sink distributions for the three scalars in space and time thereby adding to the uniqueness of the set-up. The measured and modelled fractional contributions to the momentum flux show that sweep events dominate over ejections in agreement with prior studies conducted in the roughness sublayer. For scalar fluxes, ejections dominate the turbulent fluxes over sweeps. While ejective motions persist longer for momentum transport, sweeping events persist longer for all three scalars. Third-order cumulant expansions describe many of the results detailed above, and the results are surprising given the highly non-Gaussian distribution of CH_4 turbulent fluctuations. Connections between the asymmetric contributions of sweeps and ejections and the flux-transport term arising in scalar turbulent-flux-budget closure are derived and shown to agree reasonably well with measurements. The proposed model derived here is much simpler than prior structural models used to describe laboratory experiments. Implications of such asymmetric contributions on, (i) the usage of the now proliferating relaxed-eddy-accumulation method in turbulent flux measurements, (ii) the constant-flux assumption, and (iii) gradient-diffusion closure models are presented.

Keywords Closure models · Cumulant expansion · Ejections and sweeps · Methane flux · Relaxed eddy accumulation

✉ Olli Peltola
olli.peltola@helsinki.fi

Extended author information available on the last page of the article

⌀ Springer

1 Introduction

The role of peatlands in climate science is rarely disputed given their contribution to methane (CH_4) generation (Walter and Heimann 2000; Mattson and Likens 1990). Anaerobic conditions in the soil result in CH_4 production and subsequent transport to the surface by diffusion in the water phase and in the gas phase through vegetation stems and ebullition describing sporadic bubble release from sediments (Whalen 2005). The latter two mechanisms, especially ebullition, lead to spatially patchy sources of CH_4 at the land–atmosphere interface that differ from their water vapour (H_2O) and carbon dioxide (CO_2) counterparts. The detailed signature of such spatial heterogeneity in CH_4 sources on turbulent CH_4 concentration fluctuations and concomitant turbulent transport into the atmosphere has rarely been considered and frames the scope of the work described herein.

In the high-Reynolds-number turbulent boundary layer, coherent structures with large turbulent-flux-bearing events (Cantwell 1981) have been conventionally classified as one of two types: ejections and sweeps (Robinson 1991). In momentum transport, these events are routinely detected by conditional sampling using quadrant analysis (Wallace et al. 1972; Willmarth and Lu 1972; Antonia and Atkinson 1973; Lu and Willmarth 1973; Antonia 1981). Ejection–sweep statistics and their contribution to momentum transport have been extensively investigated for smooth and rough walls (Nakagawa and Nezu 1977; Raupach 1981) at different Reynolds numbers (Priyadarshana and Klewicki 2004); canopy cover (Finnigan 1979; Shaw et al. 1983; Maitani and Ohtaki 1987; Su et al. 1998; Poggi et al. 2004a, b; Watanabe 2004; Cava et al. 2006; Thomas and Foken 2007; Yue et al. 2007); stratified atmospheric flows over uniform vegetated surfaces (Katul et al. 1997b; Li and Bou-Zeid 2011); complex terrain covered by vegetation (Baldocchi and Meyers 1988; Poggi and Katul 2007; Francone et al. 2012); the urban roughness sublayer (Rotach 1993; Moriwaki and Kanda 2006) and street canyons (Wang et al. 2014); the convective boundary layer (Wyngaard and Moeng 1992; Ghannam et al. 2017; Salesky et al. 2017); the marine boundary layer (Katsouvas et al. 2007), air-water exchange (Variano and Cowen 2013), and flow below ice-sheets (Fer et al. 2004), to list a few examples. A review of the history, development, usage, and novel extensions of quadrant analysis and conditional sampling in turbulence is presented elsewhere (Wallace 2016).

Links between quadrant analysis and Reynolds-averaged turbulence modelling was achieved using Gram–Charlier expansions (Frenkiel and Klebanoff 1967, 1973) by connecting the asymmetry in ejecting and sweeping motions to turbulent-flux-transport terms. Such cumulant expansion methods (CEMs) allow one to study the degree to which higher-order (higher than second order) cumulants are able to explain the excursions of the observed probability density function (PDF) from Gaussian distribution, since by definition for a Gaussian distribution only the first two cumulants (i.e. mean and variance) differ from zero. When low-order cumulants suffice to describe the joint PDF of the components of velocity statistics (Antonia and Atkinson 1973), the turbulent kinetic energy (TKE) can be linked to sweeping and ejecting motions via (Raupach 1981)

$$F_{TKE} = \frac{1}{2}\overline{w'(u'^2 + v'^2 + w'^2)} = \Delta S_o \left(a_1 \sigma_u^2 \sigma_w + a_2 \sigma_w^3 \right), \tag{1}$$

where F_{TKE} is the vertical transport of TKE, u', v', and w' are the turbulent velocity fluctuations in the longitudinal (or x), lateral (or y), and vertical (or z) directions, respectively, $\Delta S_o \in [-1, 1]$ signifies the relative contributions of sweeps (defined here as $\Delta S_o > 0$) and ejections (defined here as $\Delta S_o < 0$) to the turbulent momentum flux $\overline{w'u'}$, a_1, and a_2 are constants determined from experiment, $\sigma_s^2 = \overline{s'^2}$ is the variance of any turbulent flow variable

s' (i.e. s' includes velocity and scalar concentration c'), and primed quantities are excursions from their time-averaged state indicated by the overline. The definition for ΔS_o is given later in Sect. 3. The ΔS_o term can reverse the sign of F_{TKE} to or from the surface depending on the type of coherent motion that dominates the momentum transport. Equation 1 also deviates from classical gradient-diffusion schemes conventionally used to close triple moments through gradients in second moments (Launder et al. 1975). Such gradient-diffusion closures of triple moments remain the cornerstone of many operational meso-scale models such as the Weather Research and Forecasting (WRF) model described elsewhere (Mellor and Yamada 1982).

Sweep–ejection statistics and their contribution to the transport of a scalar c, especially for scalars other than temperature, have received comparatively less attention when compared to momentum transport (Wallace 2016). The analogous sweep–ejection statistics have been analyzed using quadrant analysis and links to the scalar flux-transport term $F_T = \overline{w'w'c'}$ have been offered in analogy to the much studied momentum flux. The F_T term arises in the turbulent-scalar-flux budget (Nagano and Tagawa 1990) in analogy to momentum transport (Nakagawa and Nezu 1977). In a neutrally-stratified stationary and planar-homogeneous flow lacking subsidence, the budget for the scalar flux $\overline{w'c'}$ yields

$$0 = -\sigma_w^2 \frac{\mathrm{d}\overline{C}}{\mathrm{d}z} - \frac{\mathrm{d}F_T}{\mathrm{d}z} - \overline{c'\frac{\mathrm{d}p'}{\mathrm{d}z}}, \tag{2}$$

where c' is, as defined before, the turbulent concentration of a scalar entity (i.e. CH_4, H_2O, and CO_2) characterized by a mean $\overline{C}$, and p' is the pressure fluctuation due to turbulence. The right-hand side of Eq. 2 describes a balance between three terms: a turbulent flux production arising from the action of a mean-squared turbulent turnover velocity (i.e. σ_w^2) on the mean scalar concentration vertical gradient, transport by turbulence (i.e. $\mathrm{d}F_T/\mathrm{d}z$), and pressure–scalar interaction that acts to de-correlate w' from c' and is known to be far more efficient as a destruction process when compared to molecular terms (Katul et al. 2013). As a model of maximum simplicity, the case where the pressure–scalar interaction is closed using only the slow part of a linear Rotta scheme is considered. This closure yields an expression for $\overline{w'c'}$ given by

$$\overline{w'c'} = -\frac{\tau}{C_R}\left(\sigma_w^2\frac{\mathrm{d}\overline{C}}{\mathrm{d}z} + \frac{\mathrm{d}F_T}{\mathrm{d}z}\right), \tag{3}$$

where τ is a relaxation time scale inferred from TKE and its mean dissipation rate, and C_R is the Rotta constant. In analogy to momentum, sweeps and ejections are also expected to govern the sign and magnitude of F_T, which is the 'parent term' responsible for the failure of gradient-diffusion theory across many flows (Corrsin 1975; Deardorff 1978).

To what degree the source–sink spatial inhomogeneity at the surface that is expected for CH_4 (but less so for scalars such as CO_2 or H_2O) affects connections between ejecting and sweeping motions and F_T is far from resolved, and frames the overall objective of the work reported here. To bring this point into sharper focus, the measured normalized PDFs of the time series of CH_4 ($s = CH_4$), H_2O ($s = H_2O$), CO_2 ($s = CO_2$) concentrations, and vertical velocity ($s = w$) collected above a peatland (to be described later) are shown in Fig. 1. It is evident that the *PDF* values of CH_4 concentration deviate appreciably from Gaussian, whereas the *PDF* values of the remaining scalars and vertical velocity component do not and appear reasonably described by the lower-order CEMs. In fact, Fig. 1 demonstrates that even fourth-order cumulant corrections to Gaussian distribution appear insufficient to describe the CH_4 concentration fluctuation *PDF* values, whereas third- or fourth-order CEMs appear
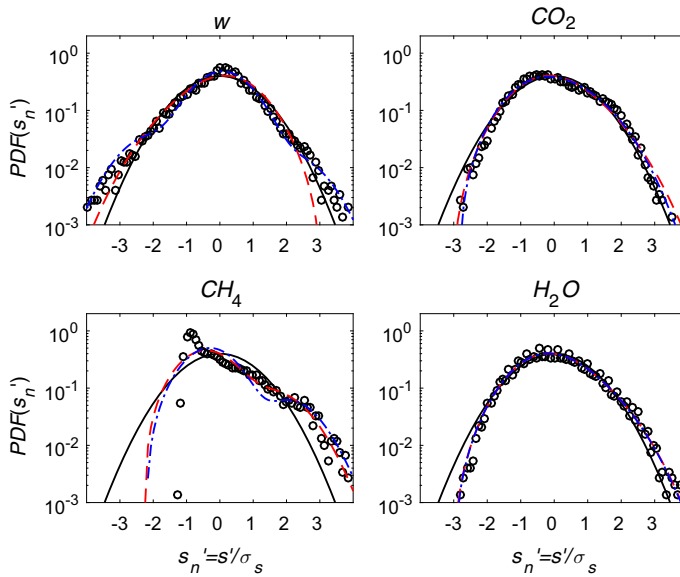
Fig. 1 Measured (symbols) and modelled (lines) probability density function (PDF) using Gaussian (solid), third-order cumulant expansion (red-dashed), and fourth-order cumulant expansion (blue-dot) for vertical velocity (top-left), CO_2 concentration (top right), CH_4 concentration (bottom left), and H_2O concentration (bottom right). The equations describing the third- and fourth-order cumulative expansion method as a function of the skewness and flatness factors employed here are described elsewhere (Nakagawa and Nezu 1977). For comparisons, all time series are normalized to zero-mean and unit variance. The series shown was collected around midnight on July 22 2013 for near-neutral atmospheric stability (stability parameter $z/L_o = 0.02$, where z is the height from the surface and L_o is the Obukhov length). Note the large deviations from a Gaussian shape for the CH_4 concentration

adequate to describe the *PDF* values of vertical velocity and the remaining turbulent scalar concentration statistics.

To address the overall objective in a systematic way, a guiding question can now be stated as follows: to what degree can the lower-order CEMs describe transport efficiency and the relative importance of sweeps and ejections to momentum, CH_4, CO_2 and H_2O fluxes across differing atmospheric thermal stratification regimes above a peatland? The aforementioned quantities such as transport efficiency and relative flux contributions due to sweeping and ejecting motions are expected to be sensitive to the joint PDFs between w' and the remaining flow variables, hereafter referred to as $JPDF(w', s')$, instead of the uni-variate *PDF* values shown in Fig. 1. The practical consequences of the findings here on, (i) the usage of the now proliferating relaxed-eddy-accumulation method in turbulent-flux measurements of trace gases, (ii) the constant-flux assumption employed in virtually all flux-monitoring field experiments, and (iii) gradient-diffusion closure models are discussed.

2 Experiment

The measurements were conducted above a boreal oligotrophic fen at Siikaneva in southern Finland (61°50′N, 24°12′E, 162 m a.s.l.) described elsewhere (Rinne et al. 2007). Briefly, the instrumentation located on a meteorological tower consisted of an ultrasonic anemometer (USA-1, Metek GmbH) that measures the three velocity components and virtual temperature,

an infrared gas analyzer (LI-7000, Licor Inc.) that measures the H_2O and CO_2 concentration fluctuations, and an off-axis integrated cavity output spectroscopic gas analyzer (FMA, Los Gatos Research) that measures CH_4 concentration fluctuations. The CH_4 gas analyzer performance has been checked against other precision systems and was found to agree with their performances (Peltola et al. 2013). Instruments were placed at $z = 2.8$ m above the surface with a 0.2-m vertical separation distance between the gas analyzer inlets and the anemometer. The site is flat but microtopographic variations do exist along with a relatively patchy vegetation cover characterized by a mean height of about 0.3 m. Also, a few open-water ponds exist around the meteorological tower depending on the hydrological state of the peatland.

All time series were sampled at 10 Hz and turbulent flow statistics were computed over a 30-min interval. The period considered here is from June to August 2013, which matches the annual peak in CH_4, CO_2 and energy fluxes observed at the site. The experiment resulted in 4416 runs, each of 30-min duration. Double rotation (i.e. $\overline{w} = \overline{v} = 0$) was employed to determine the mean flow for each 30-min run when computing velocity statistics, turbulent momentum and scalar fluxes. Gas mixing ratios were converted to be relative to dry air using H_2O data from the LI-7000 analyzer. This is also a viable approach for CH_4 mixing ratio measured with the FMA gas analyzer, since the two analyzers shared the main inlet line (Peltola et al. 2013). Because of delays between measured c' and w', a maximum cross-correlation analysis was used to compute the lag time for each run. The lag time was estimated for each gas within predefined windows set by the air-sampling flow rate, tube length and diameter. The magnitude of high-frequency loss persistent for all measurements made with closed-path analyzers was also estimated. However, any correction for the loss was neglected herein, since it was deemed to have a negligible effect on the results based on an analysis with a smaller set of data that was corrected with the approach developed by Nordbo and Katul (2013). Stationary checks (Foken and Wichura 1996) and insufficient turbulent mixing (friction velocity $u_* < 0.2$ m s^{-1}) were used as quality criteria to filter relevant runs out of the analysis, as is commonly recommended in flux-monitoring protocols (Mammarella et al. 2016). Additionally, periods when the measurement devices malfunctioned were removed prior to analysis. Out of the 4416 runs, 1430 runs passed all these filters and are used here. Throughout, the effects of buoyancy on the flow statistics are quantified using the atmospheric stability parameter $\zeta = z/L_o$, where L_o is the Obukhov length (Obukhov 1971; Foken 2006).

3 Method of Analysis

We rely heavily on quadrant analysis of the measured turbulence data and compare these results with analytically-derived expressions obtained using cumulant expansion methods. Ejecting and sweeping motions are delineated using quadrant analysis mathematically illustrated for momentum transport here. In quadrant analysis, scatter plots are formed by two turbulent flow variables (w' and u') with quadrants defined in a Cartesian plane having an abscissa w' and an ordinate u' as follows: quadrant 1 (or Q1) labelled as outward interaction for which $w' > 0$ and $u' > 0$, quadrant 2 (or Q2) labelled as sweeps for which $w' < 0$ and $u' > 0$, quadrant 3 (or Q3) labelled as inward interaction for which $w' < 0$ and $u' < 0$, and quadrant 4 (or Q4) labelled as ejections for which $w' > 0$ and $u' < 0$. Because $\overline{u'w'}$ is negative, Q2 and Q4 are presumed to be the main or direct momentum-flux transporting motions, whereas Q1 and Q3 are presumed to be counter or indirect momentum-flux contributors as they reside in quadrants with fluxes opposite in sign to $\overline{u'w'}$. For scalars, when
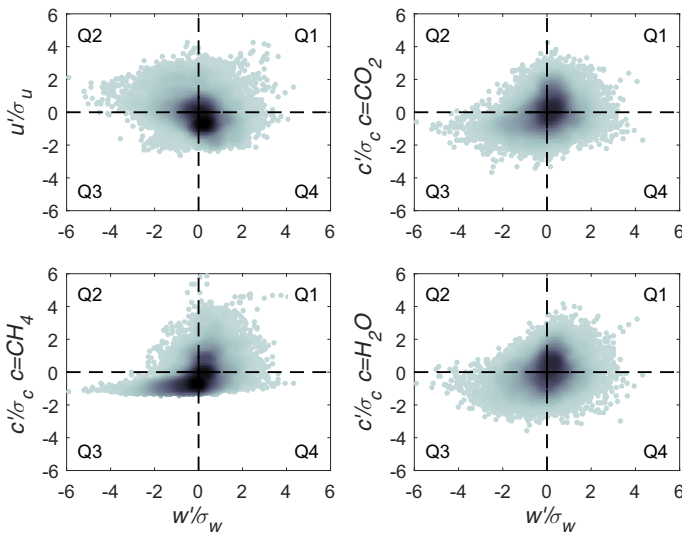
Fig. 2 Sample quadrants for momentum, CO_2, CH_4, and H_2O turbulent fluxes for the same run used in Fig. 1. Conventionally, sweeps and ejections are associated with events in quadrants 2 and 4, respectively for $\overline{w'u'} < 0$ and $\overline{w'c'} < 0$ (Note that this is opposite to Raupach (1981)). When the turbulent flux $\overline{w'c'} > 0$, sweeps and ejection events become associated with quadrants 3 and 1, respectively. Note the different scatter in CH_4 quadrants when compared to H_2O and CO_2. Colour denotes the density of the point cloud

the turbulent flux $\overline{w'c'} > 0$, sweeps and ejection events become associated with quadrants 3 and 1, respectively.

Examples of quadrants formed by w' and s' for $s' = u'$ and $s' = c'$ with c' being the concentration fluctuations for CO_2, CH_4, H_2O are shown in Fig. 2 for the same night-time run featured in Fig. 1. Here, $\overline{w'u'} < 0$ and Q2 and Q4 are the main contributors to the momentum flux. For c', $\overline{w'c'} > 0$ for all three scalars in this 30-min run and Q1 (ejection) and Q3 (sweep) become the main contributors to the turbulent flux. The sign of $\overline{w'c'}$ can vary from run-to-run, especially for CO_2. The quadrant differences in ejection–sweep transport between CH_4 and the remaining flow variables are rather striking, which is one of our main motivating points.

By expanding a Gaussian distribution with Gram–Charlier expansions (Frenkiel and Klebanoff 1967, 1973) it is possible to evaluate how well third- or higher-order moments explain the non-Gaussian character of turbulence observations (shown, e.g., in Figs. 1 and 2). In short, for a Gaussian distribution only the first two cumulants (i.e. mean and variance) differ from zero; likewise only the first two moments may vary and higher moments (e.g. skewness and kurtosis) are fixed. A third-order cumulant expansion of a univariate Gaussian PDF allows the third cumulant to differ from zero, along with a non-constant third moment (i.e. skewness). Similar cumulant expansion can be done also for bivariate probability distributions (i.e. joint PDFs). Such expansions are often used to study, e.g., the role of coherent structures on Reynolds shear stress (Raupach 1981) and scalar transport (Katul et al. 1997b) in the turbulent boundary layer and are also used herein.

One measure that characterizes the indirect ($F_{Indirect}$, inward and outward interaction) versus direct (F_{Direct}, ejections and sweeps) contributions to turbulent fluxes is the transport efficiency given by Wyngaard and Moeng (1992)

$$e_T = 1 - \left| \frac{\frac{\langle \overline{w'u'} \rangle|_1 + \langle \overline{w'u'} \rangle|_3}{\langle \overline{u'w'} \rangle}}{\frac{\langle \overline{w'u'} \rangle|_2 + \langle \overline{w'u'} \rangle|_4}{\langle \overline{u'w'} \rangle}} \right| = 1 - \left| \frac{F_{Indirect}}{F_{Direct}} \right|, \tag{4}$$

where $\langle \overline{w'u'} \rangle|_i / \langle \overline{u'w'} \rangle$ is the flux fraction in quadrant i ($i = 1, 2, 3, 4$). When the joint PDF of u' and w' is Gaussian, then (Wyngaard and Moeng [1992])

$$e_T = \frac{2\pi \, |R_{uw}|}{\pi \, |R_{uw}| + 2\sqrt{1 - R_{uw}^2} + 2|R_{uw}| \sin^{-1}(|R_{uw}|)}, \tag{5}$$

where $R_{uw} = \overline{u'w'}/(\sigma_u \sigma_w)$ is the correlation coefficient between w' and u'. A convenient measure that characterizes the flux fraction due to sweeps and ejections (i.e. ΔS_o) is given by Raupach ([1981])

$$\Delta S_o = \frac{\langle \overline{w'u'} \rangle|_2 - \langle \overline{w'u'} \rangle|_4}{\langle \overline{u'w'} \rangle}, \tag{6}$$

where $< \overline{w's'} >_i$ sums events in quadrant i. Note that here Q2 corresponds to sweeps and Q4 to ejections, which is opposite to the definition in Raupach ([1981]). Sweeps dominate the transport when $\Delta S_o > 0$ and ejections are more important when $\Delta S_o < 0$. To link ΔS_o with turbulence closure modelling, a third-order cumulant expansion to $JPDF(w', u')$ was proposed by Raupach ([1981]),

$$\Delta S_o = \frac{M_{11} + 1}{M_{11}\sqrt{2\pi}} \left[\frac{2C_1}{(1 + M_{11})^2} + \frac{C_2}{1 + M_{11}} \right], \tag{7}$$

where C_1 and C_2 are given by

$$C_1 = \left(1 + M_{11}\right)\left[\frac{1}{6}(M_{03} - M_{30}) + \frac{1}{2}(M_{21} - M_{12}) \right], \tag{8a}$$

$$C_2 = -\left[\frac{1}{6}(2 - M_{11})(M_{03} - M_{30}) + \frac{1}{2}(M_{21} - M_{12}) \right], \tag{8b}$$

$$M_{ij} = \frac{\langle \overline{w'^i u'^j} \rangle}{\sigma_w^i \sigma_u^j}. \tag{8c}$$

The M notation is convenient to use here when describing different statistical (mixed) moments. For instance M_{11} defines the correlation coefficient, M_{30} or M_{03} define individual skewnesses of w' and any flow variable s', and M_{12} (associated with turbulent transport of variance) and M_{21} (associated with turbulent transport of flux) define higher-order mixed moments. The mixed moments M_{12} and M_{21} have been shown elsewhere (Katul et al. [1999a], [2006]) to contribute more to ΔS_o than to M_{03} and M_{30} allowing for a further simplification

$$\Delta S_o \approx \frac{1}{2M_{11}\sqrt{2\pi}} \left[M_{21} - M_{12} \right], \tag{9}$$

which is hereafter referred to as an incomplete CEM. The CEM and incomplete CEM are derived for quadrants 2 and 4 when $\overline{w's'} < 0$. To apply both CEM and incomplete CEM to cases where $\overline{w's'} > 0$, a sign transformation can be applied (reverse sgn(c')) as discussed elsewhere (Katul et al. [1999a]). A large corpus of experiments on momentum transport over smooth and differing types of roughness elements suggests that $M_{12} = b_{uw} M_{21}$ across the entire boundary layer, where $b_{uw} \approx -1$ as presented elsewhere (Raupach [1981]). A value of $b_{uw} \approx -0.6$ was reported for flows within and just above dense canopies across a wide range

of thermal stratification conditions (Cava et al. 2006). If these findings are extrapolated to scalar transfer here, and also noting that $M_{21} = F_\text{T}/(\sigma_w^2 \sigma_c)$, then an expression for F_T can be derived from Eq. 9 and formulated as

$$F_\text{T} = \frac{2\sqrt{2\pi}}{1 - b_{wc}} \sigma_w^2 \sigma_c R_{wc} \Delta S_o, \tag{10}$$

which is analogous to the equation for the vertical transport of TKE (i.e. Eq. 1). This expression can be further used to formulate Eq. 3 as

$$\overline{w'c'} = -\frac{\tau}{C_R} \left(\sigma_w^2 \frac{d\overline{C}}{dz} + \frac{2\sqrt{2\pi}}{1 - b_{wc}} \frac{d}{dz} \sigma_w^2 \sigma_c R_{wc} \Delta S_o \right). \tag{11}$$

Equation 11 shows how ΔS_o (in magnitude and sign) perturbs mean gradient-diffusion closure for the scalar turbulent fluxes. Even when gradient-diffusion closure applies, differences in ΔS_o across scalars may explain why turbulent Schmidt numbers differ from unity or among scalars (Li et al. 2015; Katul et al. 2016). These are several reasons why the ΔS_o comparisons across scalars (e.g. CH_4 versus CO_2 and H_2O) are warranted. For near-Gaussian flow statistics, $\Delta S_o = 0$ and gradient-diffusion arguments apply. However, $\Delta S_o = 0$ may arise due to factors other than Gaussianity as shown later for CH_4 turbulent fluxes.

In analogy to ΔS_o, the fractional duration D_i for which the flow resides in quadrant Q_i can be determined, and the fractional duration difference between sweeps and ejections can be computed from $\Delta T_f = D_2 - D_4$. For a skewed PDF for u' characterized by a skewness M_{03} but near-Gaussian w', $\Delta T_f = M_{03}/(3\sqrt{2\pi})$ as derived elsewhere (Katul et al. 1999a). Hence, the sign of ΔT_f is dictated by the sign of the skewness of a flow variable. For near-Gaussian scalar concentration fluctuations, $\Delta T_f \approx 0$ and the flow resides equally in ejective and sweeping quadrants.

4 Results

The aforementioned methods are now employed so as to compare the performance of the CEM and incomplete CEM to the data. Figure 3 features the ΔS_o comparison between CEM (Eq. 7) and quadrant analysis (Eq. 6) for momentum and the three scalars. Both the CEM and incomplete CEM reproduce the quadrant-analysis-estimated ΔS_o for momentum and all three scalars and hence are able to explain the observed imbalance between ejections and sweeps to momentum and scalar transport. For clarity, only the results from the CEM analysis are shown in Fig. 3. While this finding may not be surprising for momentum, H_2O, and CO_2 concentration fluctuations given their near-Gaussian behaviour, it remains surprising for CH_4 given its significant non-Gaussian character (Fig. 1).

For momentum, sweeps dominate the turbulent flux whereas ejections dominate the time fraction (Fig. 4). This appears consistent with roughness sublayer measurements from wind-tunnel (Raupach 1981) and numerous vegetated and urban-canopy flow studies (Finnigan 1979; Shaw et al. 1983; Maitani and Ohtaki 1987; Rotach 1993; Katul and Albertson 1998; Finnigan 2000; Poggi et al. 2004a; Cava et al. 2006; Thomas and Foken 2007; Yue et al. 2007) instead of atmospheric surface (or inertial) layer (ASL) measurements (Raupach 1981; Poggi et al. 2004a; Li and Bou-Zeid 2011). For a near-neutral ASL, the momentum $\Delta S_o \approx 0$ while undergoing transition from $\Delta S_o > 0$ within the roughness sublayer to $\Delta S_o < 0$ in the outer layer, as reported from wind-tunnel experiments (Raupach 1981) and surface-layer measurements (Katul et al. 1997b, 2006; Li and Bou-Zeid 2011). The effects of thermal
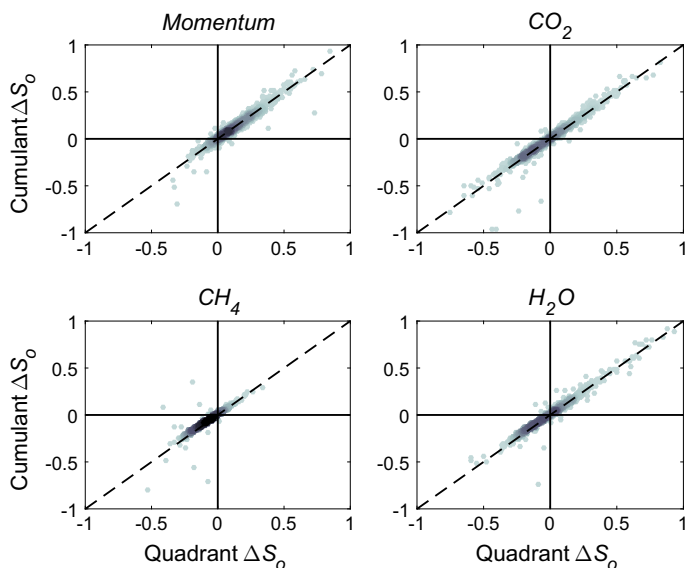
Fig. 3 Comparison between quadrant analysis measured and modelled ΔS_o by CEM for momentum transport (top left), CO_2 flux (top right), CH_4 flux (bottom left), and H_2O flux (bottom right) for all 30-min runs. Sweeps dominate when $\Delta S_o > 0$ while ejections dominate when $\Delta S_o < 0$. The one-to-one lines are shown. The results are virtually identical when repeating the comparison with ICEM instead of CEM. Colour denotes the density of the point cloud

stratification in the ASL have been shown to affect the sweep–ejection contributions to turbulent fluxes, with ejections becoming more dominant for strongly unstable conditions (Katul et al. 1997b; Li and Bou-Zeid 2011; Salesky et al. 2017). Similar unstable thermal stratification effects on ΔS_o have been reported in the roughness sublayer of urban (Moriwaki and Kanda 2006) and vegetated canopies (Maitani and Ohtaki 1987). In the case of all three scalars, ejections appear to dominate the turbulent fluxes consistent with many canopy-sublayer and surface-layer flows. For CH_4 in particular, ΔS_o appears surprisingly less variable when compared to the other scalars.

Figure 4 presents the fractional duration difference between sweeps and ejections ΔT_f predicted from longitudinal velocity component and scalar concentration skewness against estimates from quadrant analysis for momentum and the three scalars. The agreement between modelled and quadrant analysis estimated ΔT_f is again reasonable suggesting that the lower-order CEMs (mainly M_{03}) are sufficient to capture the key statistical features of the ejective and sweeping motions. Because sources and sinks at the surface primarily dictate the sign of the skewnesses (e.g. negative for momentum, positive for CH_4 and H_2O, fluctuates for CO_2), sweeping phases are expected to dominate the fractional time for CH_4 and H_2O transport and ejective phases for momentum transport. Naturally, peatlands can be sources or sinks for CO_2 depending on the environmental conditions and the plant responses to them. When the results depicted in Figs. 3 and 4 are taken together, they suggest that sweeping motions may be more prevalent but ejective motions more efficient for CH_4 (and to a lesser extent H_2O) transport given the large bursts in c'. If these large CH_4 'bursts' are associated with spatial and temporal variability of the ebullition process, then ebullition undeniably affects how sweeping and ejective coherent motions contribute to turbulent CH_4 fluxes.
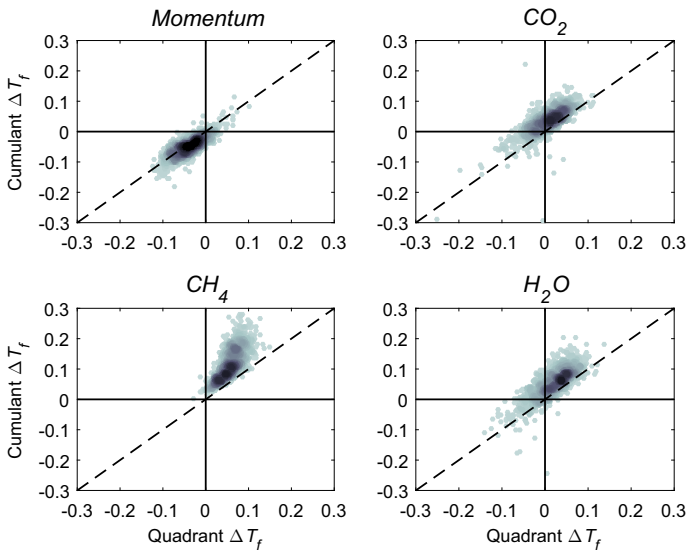
Fig. 4 Comparison between quadrant analysis measured and modelled fractional duration difference between sweeps and ejections (ΔT_f) using only M_{03} values for momentum transport (top left), CO_2 flux (top right), CH_4 flux (bottom left), and H_2O flux (bottom right) for all 30-min runs. When $\Delta T_f > 0$ sweeps dominate and when $\Delta T_f < 0$ ejections dominate the duration. The one-to-one lines are shown. Colour denotes the density of the point cloud
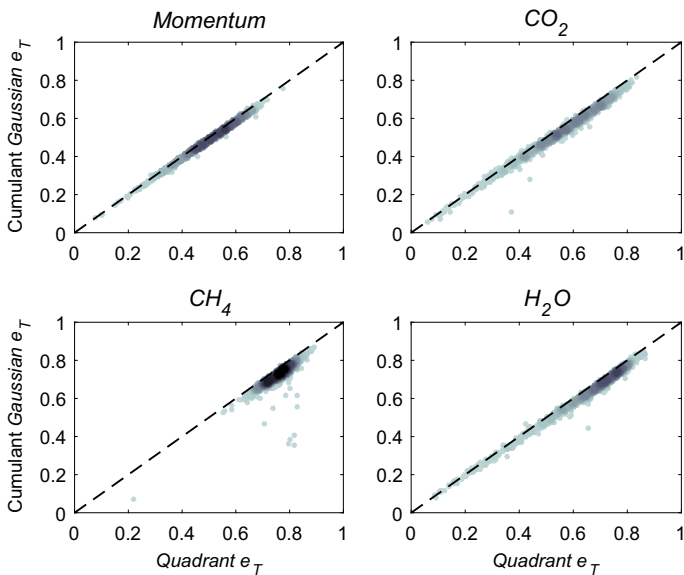

Fig. 5 Comparison between quadrant analysis measured and modelled transport (e_T) using joint Gaussian distribution for momentum transport (top left), CO_2 flux (top right), CH_4 flux (bottom left), and H_2O flux (bottom right). The one-to-one lines are shown. Colour denotes the density of the point cloud
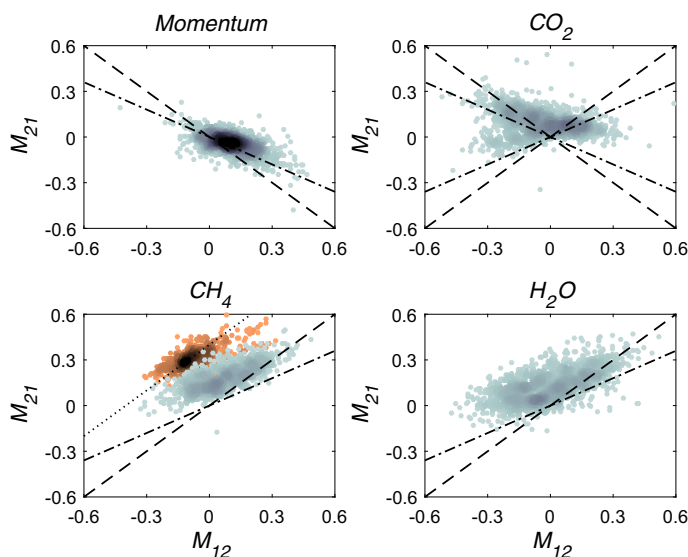
Fig. 6 Comparison between measured $M_{12} = \overline{w's's'}/(\sigma_w\sigma_s^2)$ (normalized vertical turbulent transport of variance) and $M_{21} = \overline{w'w's'}/(\sigma_s\sigma_w^2)$ (normalized vertical turbulent transport of flux) for momentum (top left), CO_2 (top right), CH_4 (bottom left), and H_2O (bottom right). The $M_{21} = M_{12}$ (dashed) and $M_{21} = 0.6M_{12}$ (dash-dot) lines (adjusted by the sign of the flux) are shown as reported from wind-tunnel experiments (Raupach 1981) and canopy sublayer measurements (Katul et al. 1999a; Katul and Albertson 1998; Poggi et al. 2004a; Cava et al. 2006). For CH_4 the additional dotted line shows the one-to-one line with adjusted intercept. Colour denotes the density of the point cloud. For CH_4 data from wind directions 260°–040° are shown with the brown colour

The transport efficiency (e_T) inferred from quadrant analysis is also reasonably reproduced by a joint Gaussian PDF as shown in Fig. 5. The transport efficiencies for momentum, CO_2, and H_2O span reasonable ranges reported elsewhere for ASL flow (Li and Bou-Zeid 2011; Francone et al. 2012). For CH_4, contributions to e_T from $F_{Indirect}$ are much smaller than from F_{Direct}, hence CH_4 has a relatively high e_T throughout the analyzed dataset. In fact, $F_{Indirect}$ contributions to e_T are smallest for CH_4 among all flow variables analyzed suggesting that direct transport dominates CH_4 fluxes. Interestingly, F_{Direct} contributions to e_T for CH_4 are commensurate with the most efficient 'bottom-up' diffusion process reported in the convective boundary layer from large-eddy simulation studies (Wyngaard and Moeng 1992).

Figure 6 shows that M_{12} and M_{21} appear proportionally consistent with wind-tunnel (Raupach 1981), ASL (Katul et al. 1997b), and canopy sublayer measurements (Katul et al. 1999a; Katul and Albertson 1998; Poggi et al. 2004a; Cava et al. 2006). For CO_2, both positive and negative relations are expected depending on the sign of the flux. Hence, Fig. 6 suggests an approximate relation between the transport of turbulent flux (M_{21}) and variance (M_{12}) for all scalars analyzed even when the turbulent flux reverses sign (as is the case for CO_2). These results support the derivation of Eqs. 10 and 11 where a linear dependence between M_{12} and M_{21} is assumed. For CH_4, and to a lesser degree for H_2O, two groupings of points can be observed in Fig. 6; they follow the same slope, but have a different (non-zero) intercept. These two datapoint groupings originate from different wind-direction sectors suggesting that the relation between the vertical transport of scalar variance (M_{12}) and vertical transport of scalar flux (M_{21}) depends on wind direction (or source area). It is expected that the dimensionless

vertical turbulent transport of CH_4 variance (i.e. $\overline{w'c'c'}/(\sigma_w\sigma_c^2)$) is more sensitive to spatially-intermittent ground sources (e.g. due to ebullition) than the dimensionless turbulent transport of fluxes (i.e. $\overline{w'w'c'}/(\sigma_c\sigma_w^2)$). This assertion is mainly due to the fact that spatial variability in CH_4 ground sources disproportionately affects σ_c^2, thereby increasing the denominator of M_{12} in specific wind directions. All in all, the outcome of the analysis in Fig. 6 invites development of structural models that are much simpler than those proposed by Nagano and Tagawa (1990).

5 Discussion

The implications of the small ΔS_o and large e_T values for CH_4 for measurement techniques using the relaxed-eddy-accumulation (REA) method and for turbulence modelling are now discussed. The focus is on the REA theory described elsewhere (Businger and Oncley 1990; Baker et al. 1992; Pattey et al. 1993) and its associated assumptions, not on any engineering design enhancements. Early attempts linked the non-Gaussian character of $JPDF(w', c')$ to assumptions used in the derivation of REA theory (Milne et al. 2001), which prompt further analysis and discussions herein. With regards to turbulence modelling, flux-gradient approaches and corollary Bowen ratio and aerodynamic methods all assume that the turbulent Schmidt number is the same across all scalars, and that the assumption $\overline{w'c'} \propto d\overline{C}/dz$ applies (i.e. no 'counter' or 'zero-mean' gradient flow). The role of ΔS_o on these assumptions is also discussed.

5.1 Implications to the Relaxed-Eddy-Accumulation Method

In the REA method, the turbulent flux is approximated by

$$\overline{w's'} = R_{ws}\sigma_w\sigma_s = \beta\sigma_w(S^+ - S^-), \tag{12}$$

where S^+ and S^- are the means of concentrations or velocity sampled in separate air compartments when $w' > 0$ and $w' < 0$, respectively, and β is assumed to be a constant (Businger and Oncley 1990). Key to the REA method is that $(S^+ - S^-)$ does not require high-frequency concentration sampling as S^+ and S^- can be measured off-line using precision gas chromatography or other means. The development and use of the REA method are exponentially proliferating in cases where high-frequency scalar concentration measurements are not possible or practical, such as measurements of volatile organic compounds, ammonia, isotopic compounds for carbon, ultra-fine aerosol particles, gaseous nitric acid, nitrous oxides, atmospheric sulphur and mercury to list a few (Nie et al. 1995; Beverland et al. 1996; Lamb et al. 1996; Bowling et al. 1998, 1999; Christensen et al. 2000; Gallagher et al. 2000; Nemitz et al. 2001; Schade and Goldstein 2001; Cobos et al. 2002; Ciccioli et al. 2003; Gaman et al. 2004; Graus et al. 2006; Skov et al. 2006; Grönholm et al. 2007; Bash and Miller 2008; Held et al. 2008; Thomas et al. 2008; Hensen et al. 2009; Park et al. 2010; Ren et al. 2011; Mochizuki et al. 2014). In arriving at Eq. 12, it is assumed that the slope of the regression line linking w'/σ_w to s'/σ_s is related to the correlation coefficient R_{ws} by

$$R_{ws} \approx \frac{(S^+ - S^-)/\sigma_s}{(w^+ - w^-)/\sigma_w}, \tag{13}$$

resulting in a β relation that conveniently depends on w' and is given by

$$\beta \approx \frac{\sigma_w}{(w^+ - w^-)}. \tag{14}$$

Only the probability density function $PDF(w')$ is now required to evaluate w^+ and w^- using

$$w^+ = 2 \int_0^\infty PDF(w')w'dw; \; w^- = 2 \int_{-\infty}^0 PDF(w')w'dw. \tag{15}$$

For a Gaussian distribution, $PDF(w') = (1/\sqrt{2\pi\sigma_w^2}) \exp\left[-(1/2)(w'/\sigma_w)^2\right]$, $w^+ = 2\sigma_w/(\sqrt{2\pi})$ and $w^- = -2\sigma_w/(\sqrt{2\pi})$ to yield $\beta = \beta_g = \sqrt{2\pi}/4 \approx 0.63$. A consequence of this assumption is that β must be either constant independent of flow conditions (i.e. z/L_o) or vary only with $PDF(w')$ (i.e. β can vary with flow conditions but cannot differ across scalars). The latter consequence permits the use of a reference scalar (e.g. H_2O) along with the REA measurements to determine run-to-run β variations as flow conditions change.

The main assumption of the REA method is Eq. 13 whose validity is explored in Fig. 7. Equation 13 reasonably captures the regression slope (or R_{ws}) variations across all flow variables and z/L_o values (including CH_4). However, a 15% overestimation and small variations around the regression lines are evident. A comparison was conducted to assess whether a non-linearity in $JPDF(w', c')$, as may be expected from the CH_4 quadrants shown in Fig. 2, explains this underestimation bias. One way to assess the effects of such non-linearity is to compute $(C^+ - 0)/(w^+ - 0)$ and $(0 - C^-)/(0 - w^-)$ as estimates of $(C^+ - C^-)/(w^+ - w^-)$. Here, the regression line describing s' against w' passes through the origin by definition. We found that these two slope estimates deviated by less than 1% across the entire record, which suggests that a single regression slope describes positive and negative branches of $JPDF(w', c')$.

This overestimation appears most consistent with the Gaussian $\beta = \beta_g = 0.63$ being large relative to β values reported in the literature. Typical β values (with no dead-band w' corrections) vary from 0.49–0.60 depending on the scalar (Pattey et al. 1993; Gao 1995; Katul et al. 1996; Tsai et al. 2012), with a stability dependence (Andreas et al. 1998; Ammann and Meixner 2002; Tsai et al. 2012) being reported as well as roughness sublayer effects (Ruppert et al. 2006). A recent study of β variations above an Amazonian rainforest (Zahn et al. 2016) showed even a height dependency (mean $\beta = 0.56$ in the roughness sublayer and $\beta \approx \beta_g$ well above the canopy), weak stability dependence with increased instability, and differences among scalars. Zahn et al. (2016) attributed the small β difference to scalar source–sink differences at the surface (detected by conditioning data on zenith angle as a surrogate for light penetration into the canopy).

Why some experiments report run-to-run variations in β for differing scalars and with different z/L_o values has not been satisfactorily answered. Does the atmospheric stability dependence of β reported by some experiments originate from variations in $PDF(w')$? If so, the effects of stability dependence of $PDF(w')$ alone cannot explain why β is different for differing scalars in some experiments. To progress further in answering this question, cumulant expansions beyond third-order for $JPDF(w', c')$ are required. As is shown later, both asymmetry and intermittency are now needed to delineate small differences in β across atmospheric stability conditions and scalars analyzed. Using a fourth-order CEM for the $JPDF(w', c')$, it was found elsewhere (Milne et al. 2001) that β is given by
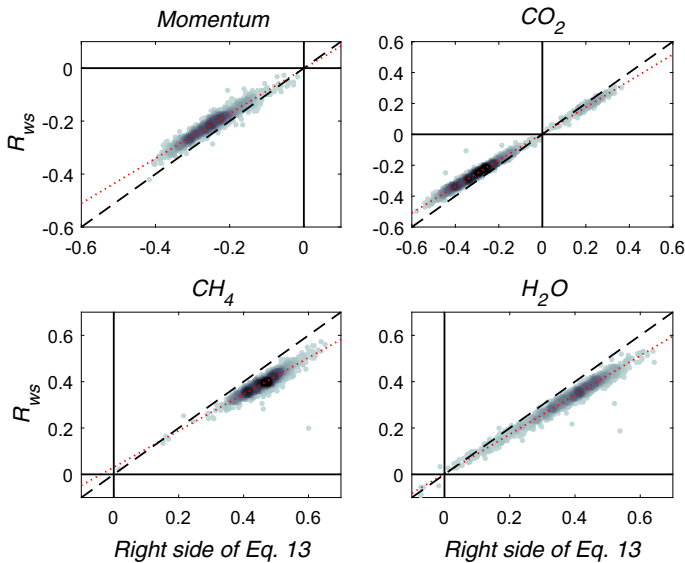
Fig. 7 Comparison between measured R_{ws} and modelled from Eq. 13 for momentum (top left), CO_2 (top right), CH_4 (bottom left), and H_2O (bottom right). The one-to-one and regression lines are shown for reference. Deviations from the one-to-one line directly impact experimentally inferred β from Eq. 12. Colour denotes the density of the point cloud

$$\beta \approx \beta_{CEM} = \frac{\frac{4}{9}\sqrt{\pi/2}}{1 + \frac{4}{27}\left(\frac{3}{4}M_{40} - M_{11}^{-1}M_{31}\right)}, \qquad (16)$$

where $M_{40} = \overline{(w'/\sigma_w)^4}$, $M_{31} = \overline{w'^3 s'}/(\sigma_w^3 \sigma_s)$, and $M_{11} = R_{ws} = \overline{w's'}/(\sigma_w \sigma_s)$ as before. To be clear, Eq. 16 is only diagnostic, not prognostic, as M_{31} and M_{11} cannot be measured in standard REA methodology. The formulation is used here because it offers a plausible explanation as to why β differs across scalars and stability conditions when scalar and momentum transport depend on the same $PDF(w')$ (or M_{40} here). Equation 16 makes clear that the source of variations in β arises from two quantities: M_{40}, which varies with the flatness factor of w', and M_{31}/M_{11}. The M_{40} is sensitive to intermittency (or on–off behaviour) of the vertical velocity only and can vary with z/L_o. However, M_{40} should be the same across all scalars for the purposes of β calculations. On the other hand, the ratio M_{31}/M_{11} reflects the role of asymmetry in w' when transporting s' as well as the effects of e_T set by M_{11} (or R_{ws}). Equation 16 is compared in Fig. 8 against β inferred using Eq. 12 for the fluxes of momentum, CO_2, CH_4, and H_2O. The mean of the measured and CEM modelled β (i.e. β_{REA} and β_{CEM}, respectively) here agree with the mean value reported by Milne et al. (2001). This value of $\beta/\beta_g = 0.56/0.63 = 0.88$ also explains much of the mean bias in the present experiment (i.e. the deviation of regression slopes from unity in Fig. 7 noted earlier). The low variability in measured and modelled β for CH_4 is rather striking when compared to the remaining flow variables in Fig. 8. This near-constancy in β for CH_4 may have been foreshadowed by the high and near-constant e_T reported in Fig. 5 but is now explored further using Eq. 16.

Equation 16 suggests that run-to-run variations in β are primarily driven by the difference in two terms: $(3/4)M_{40}$ and M_{31}/M_{11}, which are presented separately in Fig. 9 for all the studied variables. When $(3/4)M_{40} = M_{31}/M_{11}$, β is constant ($= 0.56$) independent of z/L_o
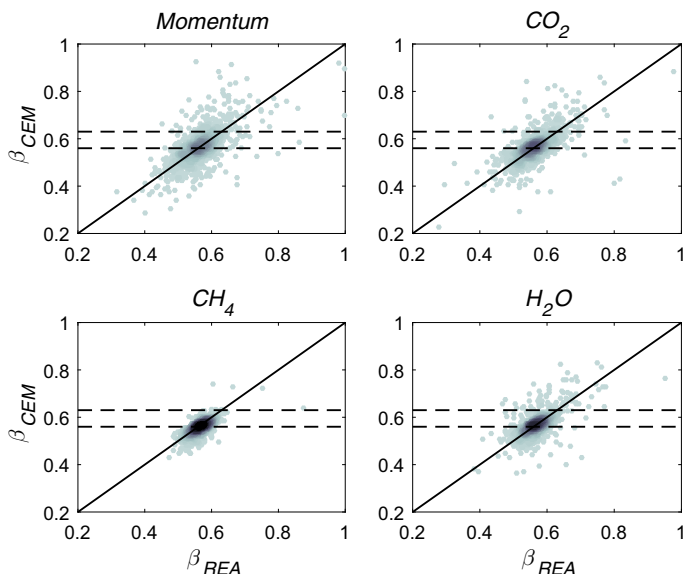
Fig. 8 Comparison between measured β_{REA} and modelled β_{CEM} from Eq. 16 for momentum (top left), CO_2 (top right), CH_4 (bottom left), and H_2O (bottom right). The one-to-one line is also shown. The horizontal lines reflect the mean β values for a Gaussian w' ($\beta_g = 0.63$) and fourth-order CEM (0.56). Colour denotes the density of the point cloud

and the scalar being analyzed. By and large, Fig. 9 suggests that M_{40} and M_{31}/M_{11} are similar in magnitude, but the terms do not fully compensate for each other when subtracted. In particular, M_{31}/M_{11} appears more dependent on variations in z/L_o than M_{40} for all variables except CH_4. Hence the difference of the two terms exhibits a z/L_o dependence and the dependence is weaker for CH_4 than for the other scalars analyzed in Fig. 9. This finding explains why small deviations in β from its expected overall mean $\beta = 0.56$ can be scalar- and stability-dependent as reported in several prior experiments. In part, M_{31}/M_{11} is sensitive to source strength, transport efficiency, and asymmetry in w' whereas M_{40} is weakly sensitive to atmospheric stability as shown here. Figure 10 presents separately how M_{31} and M_{11} vary with the transport efficiency e_T inferred from quadrant analysis. Unsurprisingly, M_{11} and e_T are quite closely related to each other as foreshadowed by a near-Gaussian $JPDF(w', s')$ prediction as discussed earlier in Fig. 5. Also, $|M_{31}|$ is connected to e_T and increases in a manner similar to M_{11} with increasing e_T. Hence, with regards to CH_4, the near-constancy of M_{31}/M_{11} is intimately connected to the high e_T (i.e. small indirect flux) separating CH_4 from other scalars. Because the indirect flux contribution is substantial for the other flow variables e_T, as well as M_{31} and M_{11}, vary, eliciting variations in β from its mean $\beta = 0.56$.

5.2 Implications to Turbulence Modelling and Constant-Flux Assumptions

From a turbulence modelling standpoint, the work here simultaneously links imbalances between sweeps and ejections through the sign of ΔS_o to, (i) the potential onset of turbulent flux variations with height that are assumed small in field experiments linking surface emission or uptake to turbulent fluxes, and (ii) deviations from K-theory and the role of non-local transport. Equation 11 can be written as a first-order ordinary differential equation given as
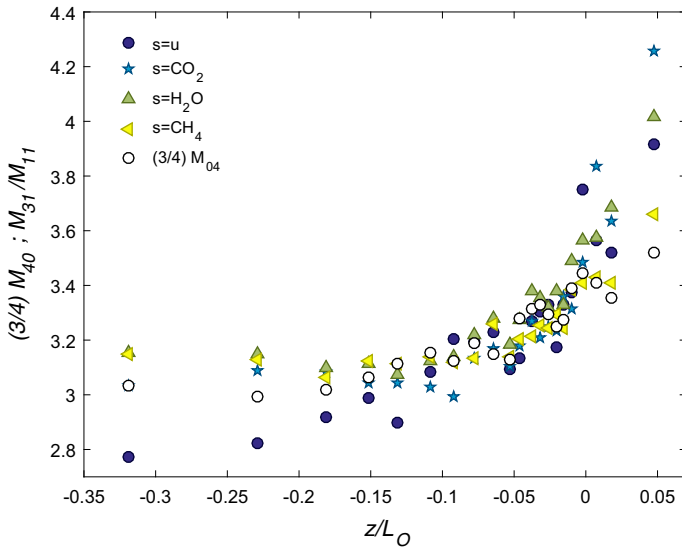
Fig. 9 Variations of (3/4) M_{40} and M_{31}/M_{11} with the stability parameter z/L_o for different flow variables. For clarity data were binned prior to plotting and bin medians are shown
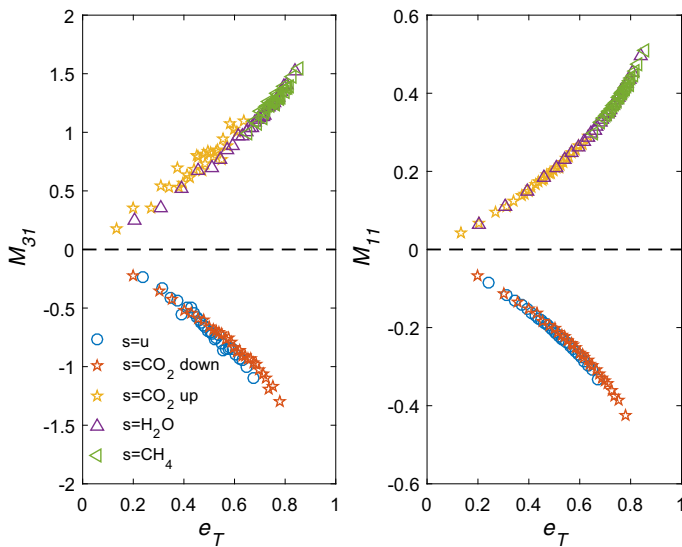

Fig. 10 Variations of M_{31} and M_{11} with quadrant analysis estimated transport efficiency e_T. For clarity data were binned prior to plotting and bin medians are shown

$$A_1(z)\frac{d\overline{w'c'}}{dz} + A_2(z)\overline{w'c'} = -\sigma_w^2\frac{d\overline{C}}{dz}, \tag{17}$$

where

$$A_1(z) = \frac{2\sqrt{2\pi}}{1 - b_{wc}}\sigma_w(z)\Delta S_o(z) \tag{18a}$$

$$A_2(z) = \frac{C_R}{\tau(z)} + \frac{dA_1}{dz}. \tag{18b}$$

When $\Delta S_o = 0$ (i.e. equal contributions to the turbulent flux from sweeps and ejections), $A_1 = 0$, $A_2(z) = C_R/\tau(z)$, and $\overline{w'c'} = -K_t(z)dC(z)/dz$, where $K_t(z)$ is the turbulent diffusivity given by $\tau(z)\sigma_w(z)^2/C_R$. That is, K-theory and corollary mean gradient methods (e.g. Bowen ratio, aerodynamic) reasonably describe turbulent fluxes. On the other hand, a finite ΔS_o can lead to a height-dependent $\overline{w'c'}$, which is problematic when interpreting turbulent fluxes as ground sources or sinks. A height-dependent ΔS_o also modifies K_t by modifying the height-dependent inverse time scale C_R/τ through dA_1/dz, thereby resulting in apparent turbulent Schmidt numbers that deviate from unity depending on the sign of $d\Delta S_o/dz$. As demonstrated by several laboratory and field experiments, the transition vertically from the roughness sublayer to the inertial layer is invariably accompanied by a height-dependent ΔS_o (Raupach 1981). Likewise, changes in thermal stratification introduce an apparent z-dependent ΔS_o through a dependence on the z/L_o, as noted elsewhere (Katul et al. 1997b; Li and Bou-Zeid 2011).

6 Conclusions

Using quadrant analysis and measured high-frequency concentration fluctuations of CH_4, CO_2, H_2O, as well as velocity components above a peatland, the following specific conclusions can be drawn:

– Sweeping motions dominate momentum transport, whereas ejective motions dominate turbulent scalar fluxes, especially CH_4. For momentum, these findings suggest that the flow statistics above the peatland are analogous to those sampled in the roughness sublayer instead of the equilibrium layer despite the fact that the turbulent measurements are conducted at some eight times the mean canopy height. Within the canopy sublayer (dense or sparse) adjacent to the canopy top, sweeps also dominate over ejections. It is conjectured that the effects of microtopography, clustering of vegetation, and open water bodies to the momentum transfer may not have been entirely blended at the measurement height. More significant is that a variable such as ΔS_o may be used in future studies to define the thickness of the roughness sublayer, which remains elusive.
– The fractional duration differences between sweeping and ejective motions can be predicted from scalar or longitudinal velocity skewness values (i.e. M_{03}) as demonstrated by third-order cumulant expansions. The sign of M_{03} is directly controlled by whether the surface acts as a source (e.g. CH_4 or H_2O) or a sink (e.g. momentum or daytime CO_2 flux) for the flow variable being analyzed.
– Some dissimilarity existed in the dimensionless vertical transport of variances and turbulent fluxes (i.e. M_{12} and M_{21}) for all flow variables. However, the two modes of transport appear reasonably correlated with each other once the sign of the turbulent flux and wind direction dependence for CH_4 are considered. The variability in M_{12} against M_{21} for CH_4 is connected to the large spatial and temporal variances in CH_4 sources (e.g. due to ebullition).
– When a fourth-order cumulant expansion is applied to the relaxed-eddy accumulation formulation, the main deviation of its key parameter β from Gaussian predictions ($\beta_g = 0.63$) is explained. Run-to-run variations in β originate from two terms: the flatness factor in vertical velocity (M_{40}) connected to intermittency and the asymmetry in velocity-scalar transport M_{31}/M_{11} linked to the transport efficiency (e_T). Variations in atmospheric

stability affect M_{31}/M_{11} more than the vertical velocity intermittency characterized by M_{40}. This differential sensitivity to atmospheric stability in M_{31}/M_{11} and M_{40} causes β to vary by some 15% (5% for CH_4) from its long-term mean predicte value at $\beta = 0.56$. The latter constant value was derived from the same cumulant expansion analysis but using averages across all runs. Individually, M_{31} and M_{11} vary with e_T uniformly across scalars but their ratio appears less variable.

– Deviations from unity in the turbulent Schmidt number or the turbulent flux variations with height have been analytically linked to the relative contributions of sweeps and ejections. These connections lead to expressions that are much simpler than earlier structural models derived from wind-tunnel and open channel flows.

A number of features can now be highlighted regarding the role of surface-flux spatial and temporal variability on scalar transport. When comparing CH_4 sources with other scalars, two points stand out that distinguish CH_4 from the other scalars: plant transport and ebullition. A heterogeneous plant distribution also affects CO_2 variability, but presumably to a lesser degree than for CH_4. To begin with, variable CH_4 emissions result in CH_4 concentration fluctuation PDFs that are quite distinct from their horizontal and vertical velocity, H_2O, and CO_2 concentration counterparts. While fourth-order cumulant expansions reasonably capture the individual velocity and the remaining scalar PDF values, they could not fully capture the CH_4 PDF values. However, a third-order cumulant expansion suffices when describing many aspects of the joint PDF such as asymmetry arising from the imbalance between sweeps and ejections. The work here also shows that the variability in CH_4 emissions from the surface result in CH_4 transport efficiencies that are less variable and much higher than those associated with momentum, H_2O, or CO_2 turbulent transport. In fact, the transport efficiency for CH_4 is commensurate with the high values reported for bottom-up diffusion in the convective boundary layer. This finding can be explained by quadrant analysis, where the CH_4 emission bursts appear to concentrate flux-bearing events in quadrants 1 and 3 (i.e. the direct flux-transporting quadrants) and minimize occurrences in quadrants 2 and 4 (the indirect flux-transporting quadrants). This result explains why β and M_{31}/M_{11} appear less variable for CH_4 when compared to the remaining flow variables.

References

Ammann C, Meixner F (2002) Stability dependence of the relaxed eddy accumulation coefficient for various scalar quantities. J Geophys Res Atmos 107(D8):ACL7-1–ACL7-9

Andreas EL, Hill RJ, Gosz JR, Moore DI, Otto WD, Sarma AD (1998) Stability dependence of the eddy-accumulation coefficients for momentum and scalars. Boundary-Layer Meteorol 86(3):409–420

Antonia R (1981) Conditional sampling in turbulence measurement. Annu Rev Fluid Mech 13(1):131–156

Antonia R, Atkinson J (1973) High-order moments of Reynolds shear stress fluctuations in a turbulent boundary layer. J Fluid Mech 58(03):581–593

Baker J, Norman J, Bland W (1992) Field-scale application of flux measurement by conditional sampling. Agric For Meteorol 62(1–2):31–52

Baldocchi DD, Meyers TP (1988) Turbulence structure in a deciduous forest. Boundary-Layer Meteorol 43(4):345–364

Bash JO, Miller DR (2008) A relaxed eddy accumulation system for measuring surface fluxes of total gaseous mercury. J Atmos Ocean Technol 25(2):244–257

Beverland I, Moncrieff J, Oneill D, Hargreaves K, Milne R (1996) Measurement of methane and carbon dioxide fluxes from peatland ecosystems by the conditional-sampling technique. Q J R Meteorol Soc 122(532):819–838

Bowling D, Turnipseed A, Delany A, Baldocchi D, Greenberg J, Monson R (1998) The use of relaxed eddy accumulation to measure biosphere-atmosphere exchange of isoprene and other biological trace gases. Oecologia 116(3):306–315

Bowling DR, Baldocchi DD, Monson RK (1999) Dynamics of isotopic exchange of carbon dioxide in a tennessee deciduous forest. Global Biogeochem Cycles 13(4):903–922. https://doi.org/10.1029/1999GB900072

Businger JA, Oncley SP (1990) Flux measurement with conditional sampling. J Atmos Ocean Technol 7(2):349–352

Cantwell BJ (1981) Organized motion in turbulent flow. Annu Rev Fluid Mech 13(1):457–515

Cava D, Katul G, Scrimieri A, Poggi D, Cescatti A, Giostra U (2006) Buoyancy and the sensible heat flux budget within dense canopies. Boundary-Layer Meteorol 118(1):217–240

Christensen C, Hummelshøj P, Jensen N, Larsen B, Lohse C, Pilegaard K, Skov H (2000) Determination of the terpene flux from orange species and Norway spruce by relaxed eddy accumulation. Atmos Environ 34(19):3057–3067

Ciccioli P, Brancaleoni E, Frattoni M, Marta S, Brachetti A, Vitullo M, Tirone G, Valentini R (2003) Relaxed eddy accumulation, a new technique for measuring emission and deposition fluxes of volatile organic compounds by capillary gas chromatography and mass spectrometry. J Chromatogr A 985(1):283–296

Cobos DR, Baker JM, Nater EA (2002) Conditional sampling for measuring mercury vapor fluxes. Atmos Environ 36(27):4309–4321

Corrsin S (1975) Limitations of gradient transport models in random walks and in turbulence. Adv Geophys 18:25–60

Deardorff J (1978) Closure of second-and third-moment rate equations for diffusion in homogeneous turbulence. Phys Fluids 21(4):525–530

Fer I, McPhee MG, Sirevaag A (2004) Conditional statistics of the Reynolds stress in the under-ice boundary layer. Geophys Res Lett. https://doi.org/10.1029/2004GL020475

Finnigan J (1979) Turbulence in waving wheat II. Structure of momentum transfer. Boundary-Layer Meteorol 16:213–236

Finnigan J (2000) Turbulence in plant canopies. Annu Rev Fluid Mech 32(1):519–571

Foken T (2006) 50 years of the Monin–Obukhov similarity theory. Boundary-Layer Meteorol 119(3):431–447

Foken T, Wichura B (1996) Tools for quality assessment of surface-based flux measurements. Agric For Meteorol 78(1–2):83–105

Francone C, Katul GG, Cassardo C, Richiardone R (2012) Turbulent transport efficiency and the ejection-sweep motion for momentum and heat on sloping terrain covered with vineyards. Agric For Meteorol 162:98–107

Frenkiel FN, Klebanoff PS (1967) Higher-order correlations in a turbulent field. Phys Fluids 10(3):507–520

Frenkiel FN, Klebanoff PS (1973) Probability distributions and correlations in a turbulent boundary layer. Phys Fluids 16(6):725–737

Gallagher M, Clayborough R, Beswick K, Hewitt C, Owen S, Moncrieff J, Pilegaard K (2000) Assessment of a relaxed eddy accumulation for measurements of fluxes of biogenic volatile organic compounds: study over arable crops and a mature beech forest. Atmos Environ 34(18):2887–2899

Gaman A, Rannik Ü, Aalto P, Pohja T, Siivola E, Kulmala M, Vesala T (2004) Relaxed eddy accumulation system for size-resolved aerosol particle flux measurements. J Atmos Ocean Technol 21(6):933–943

Gao W (1995) The vertical change of coefficient b, used in the relaxed eddy accumulation method for flux measurement above and within a forest canopy. Atmos Environ 29(17):2339–2347

Ghannam K, Duman T, Salesky ST, Chamecki M, Katul G (2017) The non-local character of turbulence asymmetry in the convective atmospheric boundary layer. Q J R Meteorol Soc 143(702):494–507

Graus M, Hansel A, Wisthaler A, Lindinger C, Forkel R, Hauff K, Klauer M, Pfichner A, Rappenglück B, Steigner D et al (2006) A relaxed-eddy-accumulation method for the measurement of isoprenoid canopy-fluxes using an online gas-chromatographic technique and PTR-MS simultaneously. Atmos Environ 40:43–54

Grönholm T, Aalto PP, Hiltunen V, Rannik Ü, Rinne J, Laakso L, Hyvönen S, Vesala T, Kulmala M (2007) Measurements of aerosol particle dry deposition velocity using the relaxed eddy accumulation technique. Tellus B 59(3):381–386

Held A, Patton E, Rizzo L, Smith J, Turnipseed A, Guenther A (2008) Relaxed eddy accumulation simulations of aerosol number fluxes and potential proxy scalars. Boundary-Layer Meteorol 129(3):451–468

Hensen A, Nemitz E, Flynn M, Blatter A, Jones S, Sørensen LL, Hensen B, Pryor S, Jensen B, Otjes R et al (2009) Inter-comparison of ammonia fluxes obtained using the relaxed eddy accumulation technique. Biogeosciences 6(11):2575–2588

Katsouvas GD, Helmis CG, Wang Q (2007) Quadrant analysis of the scalar and momentum fluxes in the stable marine atmospheric surface layer. Boundary-Layer Meteorol 124(3):335–360

Katul G, Albertson J (1998) An investigation of higher-order closure models for a forested canopy. Boundary-Layer Meteorol 89(1):47–74

Katul GG, Finkelstein PL, Clarke JF, Ellestad TG (1996) An investigation of the conditional sampling method used to estimate fluxes of active, reactive, and passive scalars. J Appl Meteorol 35(10):1835–1845

Katul G, Hsieh CI, Kuhn G, Ellsworth D, Nie D (1997a) Turbulent eddy motion at the forest-atmosphere interface. J Geophys Res Atmos 102(D12):13,409–13,421

Katul G, Kuhn G, Schieldge J, Hsieh CI (1997b) The ejection-sweep character of scalar fluxes in the unstable surface layer. Boundary-Layer Meteorol 83(1):1–26

Katul G, Poggi D, Cava D, Finnigan J (2006) The relative importance of ejections and sweeps to momentum transfer in the atmospheric boundary layer. Boundary-Layer Meteorol 120(3):367–375

Katul GG, Porporato A, Manes C, Meneveau C (2013) Co-spectrum and mean velocity in turbulent boundary layers. Phys Fluids 25(9):091,702

Katul GG, Li D, Liu H, Assouline S (2016) Deviations from unity of the ratio of the turbulent Schmidt to Prandtl numbers in stratified atmospheric flows over water surfaces. Phys Rev Fluids 1(3):034,401

Lamb B, Pierce T, Baldocchi D, Allwine E, Dilts S, Westberg H, Geron C, Guenther A, Klinger L, Harley P et al (1996) Evaluation of forest canopy models for estimating isoprene emissions. J Geophys Res Atmos 101(17):22,787–22,797

Launder B, Reece GJ, Rodi W (1975) Progress in the development of a Reynolds-stress turbulence closure. J Fluid Mech 68(03):537–566

Li D, Bou-Zeid E (2011) Coherent structures and the dissimilarity of turbulent transport of momentum and scalars in the unstable atmospheric surface layer. Boundary-Layer Meteorol 140(2):243–262

Li D, Katul GG, Zilitinkevich SS (2015) Revisiting the turbulent Prandtl number in an idealized atmospheric surface layer. J Atmos Sci 72(6):2394–2410

Lu S, Willmarth W (1973) Measurements of the structure of the Reynolds stress in a turbulent boundary layer. J Fluid Mech 60(03):481–511

Maitani T, Ohtaki E (1987) Turbulent transport processes of momentum and sensible heat in the surface layer over a paddy field. Boundary-Layer Meteorol 40(3):283–293

Mammarella I, Peltola O, Nordbo A, Järvi L, Rannik Ü (2016) Quantifying the uncertainty of eddy covariance fluxes due to the use of different software packages and combinations of processing steps in two contrasting ecosystems. Atmos Meas Tech 9(10):4915

Mattson MD, Likens GE (1990) Air pressure and methane fluxes. Nature 347:718–719

Mellor GL, Yamada T (1982) Development of a turbulence closure model for geophysical fluid problems. Rev Geophys 20(4):851–875

Milne R, Mennim A, Hargreaves K (2001) The value of the β coefficient in the relaxed eddy accumulation method in terms of fourth-order moments. Boundary-Layer Meteorol 101(3):359–373

Mochizuki T, Tani A, Takahashi Y, Saigusa N, Ueyama M (2014) Long-term measurement of terpenoid flux above a Larix kaempferi forest using a relaxed eddy accumulation method. Atmos Environ 83:53–61

Moriwaki R, Kanda M (2006) Local and global similarity in turbulent transfer of heat, water vapour, and CO_2 in the dynamic convective sublayer over a suburban area. Boundary-Layer Meteorol 120(1):163–179

Nagano Y, Tagawa M (1990) A structural turbulence model for triple products of velocity and scalar. J Fluid Mech 215:639–657

Nakagawa H, Nezu I (1977) Prediction of the contributions to the Reynolds stress from bursting events in open-channel flows. J Fluid Mech 80(01):99–128

Nemitz E, Flynn M, Williams P, Milford C, Theobald M, Blatter A, Gallagher M, Sutton M (2001) A relaxed eddy accumulation system for the automated measurement of atmospheric ammonia fluxes. Water Air Soil Pollut: Focus 1(5):189–202

Nie D, Kleindienst T, Arnts R, Sickles J (1995) The design and testing of a relaxed eddy accumulation system. J Geophys Res Atmos 100(D6):11,415–11,423

Nordbo A, Katul G (2013) A wavelet-based correction method for eddy-covariance high-frequency losses in scalar concentration measurements. Boundary-Layer Meteorol 146(1):81–102. https://doi.org/10.1007/s10546-012-9759-9

Obukhov A (1971) Turbulence in an atmosphere with a non-uniform temperature. Boundary-Layer Meteorol 2(1):7–29

Park C, Schade GW, Boedeker I (2010) Flux measurements of volatile organic compounds by the relaxed eddy accumulation method combined with a GC-FID system in urban Houston, Texas. Atmos Environ 44(21):2605–2614

Pattey E, Desjardins R, Rochette P (1993) Accuracy of the relaxed eddy-accumulation technique evaluated using CO_2 flux measurements. Boundary-Layer Meteorol 66(4):341–355

Peltola O, Mammarella I, Haapanala S, Burba G, Vesala T (2013) Field intercomparison of four methane gas analyzers suitable for eddy covariance flux measurements. Biogeosciences 10(6):3749–3765. https://doi.org/10.5194/bg-10-3749-2013

Poggi D, Katul G (2007) The ejection-sweep cycle over gentle hills covered with bare and forested surfaces. Boundary-Layer Meteorol 122:493–515

Poggi D, Katul G, Albertson J (2004a) Momentum transfer and turbulent kinetic energy budgets within a dense model canopy. Boundary-Layer Meteorol 111:589–614

Poggi D, Porporato A, Ridolfi L, Katul G, Albertson J (2004b) The effect of vegetation density on canopy sublayer turbulence. Boundary-Layer Meteorol 111:565–587

Priyadarshana P, Klewicki J (2004) Study of the motions contributing to the Reynolds stress in high and low Reynolds number turbulent boundary layers. Phys Fluids 16(12):4586–4600

Raupach M (1981) Conditional statistics of Reynolds stress in rough-wall and smooth-wall turbulent boundary layers. J Fluid Mech 108:363–382

Ren X, Sanders J, Rajendran A, Weber R, Goldstein A, Pusede S, Browne E, Min KE, Cohen R (2011) A relaxed eddy accumulation system for measuring vertical fluxes of nitrous acid. Atmos Meas Tech 4(10):2093–2103

Rinne J, Riutta T, Pihlatie M, Aurela M, Haapanala S, Tuovinen JP, Tuittila ES, Vesala T (2007) Annual cycle of methane emission from a boreal fen measured by the eddy covariance technique. Tellus B 59(3):449–457

Robinson SK (1991) Coherent motions in the turbulent boundary layer. Annu Rev Fluid Mech 23(1):601–639

Rotach MW (1993) Turbulence close to a rough urban surface part I: Reynolds stress. Boundary-Layer Meteorol 65(1):1–28

Ruppert J, Thomas C, Foken T (2006) Scalar similarity for relaxed eddy accumulation methods. Boundary-Layer Meteorol 120(1):39–63

Salesky ST, Chamecki M, Bou-Zeid E (2017) On the nature of the transition between roll and cellular organization in the convective boundary layer. Boundary-Layer Meteorol 163(1):41–68. https://doi.org/10.1007/s10546-016-0220-3

Schade GW, Goldstein AH (2001) Fluxes of oxygenated volatile organic compounds from a Ponderosa pine plantation. J Geophys Res Atmos 106(D3):3111–3123

Shaw RH, Tavangar J, Ward DP (1983) Structure of the Reynolds stress in a canopy layer. J Clim Appl Meteorol 22(11):1922–1931

Skov H, Brooks SB, Goodsite ME, Lindberg SE, Meyers TP, Landis MS, Larsen MR, Jensen B, McConville G, Christensen J (2006) Fluxes of reactive gaseous mercury measured with a newly developed method using relaxed eddy accumulation. Atmos Environ 40(28):5452–5463

Su HB, Shaw RH, Paw KT, Moeng CH, Sullivan PP (1998) Turbulent statistics of neutrally stratified flow within and above a sparse forest from large-eddy simulation and field observations. Boundary-Layer Meteorol 88(3):363–397

Thomas C, Foken T (2007) Flux contribution of coherent structures and its implications for the exchange of energy and matter in a tall spruce canopy. Boundary-Layer Meteorol 123(2):317–337

Thomas C, Martin J, Goeckede M, Siqueira M, Foken T, Law B, Loescher H, Katul G (2008) Estimating daytime subcanopy respiration from conditional sampling methods applied to multi-scalar high frequency turbulence time series. Agric For Meteorol 148(8):1210–1229

Tsai JL, Tsuang BJ, Kuo PH, Tu CY, Chen CL, Hsueh MT, Lee CS, Yao MH, Hsueh ML (2012) Evaluation of the relaxed eddy accumulation coefficient at various wetland ecosystems. Atmos Environ 60:336–347

Variano EA, Cowen EA (2013) Turbulent transport of a high-Schmidt-number scalar near an air-water interface. J Fluid Mech 731:259–287

Wallace JM (2016) Quadrant analysis in turbulence research: history and evolution. Annu Rev Fluid Mech 48:131–158

Wallace JM, Eckelmann H, Brodkey RS (1972) The wall region in turbulent shear flow. J Fluid Mech 54(01):39–48

Walter BP, Heimann M (2000) A process-based, climate-sensitive model to derive methane emissions from natural wetlands: application to five wetland sites, sensitivity to model parameters, and climate. Global Biogeochem Cycles 14(3):745–765

Wang L, Li D, Gao Z, Sun T, Guo X, Bou-Zeid E (2014) Turbulent transport of momentum and scalars above an urban canopy. Boundary-Layer Meteorol 150(3):485–511

Watanabe T (2004) Large-eddy simulation of coherent turbulence structures associated with scalar ramps over plant canopies. Boundary-Layer Meteorol 112(2):307–341

Whalen SC (2005) Biogeochemistry of methane exchange between natural wetlands and the atmosphere. Environ Eng Sci 22(1):73–94. https://doi.org/10.1089/ees.2005.22.73

Willmarth W, Lu S (1972) Structure of the Reynolds stress near the wall. J Fluid Mech 55(01):65–92

Wyngaard JC, Moeng CH (1992) Parameterizing turbulent diffusion through the joint probability density. Boundary-Layer Meteorol 60(1):1–13

Yue W, Meneveau C, Parlange MB, Zhu W, van Hout R, Katz J (2007) A comparative quadrant analysis of turbulence in a plant canopy. Water Resour Res 43:W05422. https://doi.org/10.1029/2006WR005583

Zahn E, Dias NL, Araújo A, Sá LD, Sörgel M, Trebs I, Wolff S, Manzi A (2016) Scalar turbulent behavior in the roughness sublayer of an amazonian forest. Atmos Chem Phys 16(17):11,349–11,366

Affiliations

Gabriel Katul[1,2,3] · Olli Peltola[3] · Tiia Grönholm[3] · Samuli Launiainen[4] · Ivan Mammarella[3] · Timo Vesala[3,5]

[1]   Nicholas School of the Environment, Duke University, Box 90328, Durham, NC 27708, USA

[2]   Department of Civil and Environmental Engineering, Duke University, Durham, NC 27708, USA

[3]   Institute for Atmospheric and Earth System Research/Physics, Faculty of Science, University of Helsinki, P.O. Box 68, 00014 Helsinki, Finland

[4]   Natural Resources Institute Finland, Environmental Impacts of Production, Latokartanonkaari 9, 00790 Helsinki, Finland

[5]   Institute for Atmospheric and Earth System Research/Forest Sciences, Faculty of Agriculture and Forestry, University of Helsinki, P.O. Box 27, 00014 Helsinki, Finland